JOURNAL OF MATERIALS SCIENCE 25 (1990) 2233–2244

Sintering and microstructural studies in the system $ZrO_2 \cdot TiO_2 \cdot CeO_2$

V. C. PANDOLFELLI*, M. RAINFORTH, R. STEVENS
School of Materials, Division of Ceramics, University of Leeds, Leeds LS2 9JT, UK

Tetragonal zirconia polycrystals (TZP) in the system $ZrO_2 \cdot TiO_2 \cdot CeO_2$ have been prepared from titanium and zirconium alkoxides and cerium nitrate precursors. The change in microstructure with sintering temperature in the range 1300 to 1600° C has been characterized. A fully tetragonal structure with theoretical final density has been achieved after liquid-phase sintering in the range 1350 to 1400° C for 2 h. Sintering at temperatures above 1450° C resulted in a loss of stabilizer from the matrix, by the formation of zirconium titanate and to a cerium-, titanium-rich liquid. The loss of stabilizer was such that in the temperature range 1500 to 1600° C, extensive transformation to monoclinic zirconia occurred spontaneously on cooling. The tetragonal zirconia formed after sintering at 1350° C was found to be very stable. The *c/a* ratio of the tetragonal phase in this system is higher than in any of the binary TZP systems reported in the literature. The stability of the tetragonal phase is believed to be associated with this high *c/a* ratio.

1. Introduction

Zirconia engineering ceramics have received considerable attention in recent years [1–3]. The study of the interplay between microstructure, composition and stability of each of the three polymorphs (cubic, tetragonal and monoclinic) has led to improvements in the properties of these materials, with high values of toughness being reported in the literature. Whilst an understanding of the mechanisms involved is now reasonable, further study is being conducted into new compositions which might well provide additional transformation toughened ceramics (e.g. [4]). In addition, further work on the factors controlling the nucleation and growth of the martensitic t → m transformation, and therefore the optimum toughness, is required. This paper considers both these aspects. The properties of a composition hitherto not investigated are reported and then aspects of factors controlling the stability of the tetragonal phase are discussed.

Both $ZrO_2 \cdot CeO_2$ [5] and $ZrO_2 \cdot TiO_2$ [6] phase diagrams contain extensive tetragonal phase fields. Despite this, at least 8 mol % CeO_2 is required to stabilize the tetragonal zirconia to room temperature, whilst a fully dense tetragonal polycrystal ceramic cannot be obtained in the $ZrO_2 \cdot TiO_2$ system [7].

Previous investigations of the $ZrO_2 \cdot TiO_2 \cdot CeO_2$ ternary system show that the addition of TiO_2 to $ZrO_2 \cdot CeO_2$ does not affect the stability of the tetragonal phase [8]. In the system investigated, a fully dense tetragonal zirconia polycrystal ceramic was only achieved by doping with 15 mol % CeO_2, even with the addition of up to 6 mol % TiO_2.

Because the retention of a fully tetragonal structure at room temperature is most likely with the eutectoid composition, this was chosen for the present study. A ternary phase diagram is not available for the $ZrO_2 \cdot TiO_2 \cdot CeO_2$ system and therefore a composition was formulated which kept both the $TiO_2/TiO_2 + ZrO_2$ and $CeO_2/CeO_2 + ZrO_2$ at their eutectoid ratios. Fully dense tetragonal zirconia polycrystals (TZP) have been obtained at such a composition ($77.9ZrO_2 \cdot 16.5TiO_2 \cdot 5.6CeO_2$ mol %), after sintering in the temperature range 1350 to 1400° C.

Sintering in the temperature range 1300 to 1600° C has been investigated and the microstructure generated characterized in terms of phase analysis and quantitative microanalysis.

The tetragonal phase obtained after sintering at 1350° C showed exceptionally high stability with significant transformation to the monoclinic phase occuring only after ageing 64 h at 1350° C. Because the fracture toughness of zirconia ceramics is controlled by the degree of the t → m transformation, it is important to consider the reasons for a high tetragonal stability. The present results are compared with those recently published by Bestgen *et al.* [9], and Urabe *et al.* [10], in which various artefacts from thin foil preparation for transmission electron microscopy were reported.

2. Experimental procedure

The composition of $77.9ZrO_2 \cdot 16.5TiO_2 \cdot 5.6CeO_2$ mol % was formulated to maintain the eutectoid ratios of the ZrO_2/TiO_2 and ZrO_2/CeO_2 binary systems. Powders were prepared by coprecipitation of zirconium *n*-propoxide and titanium isopropoxide in a continuously stirred aqueous solution of $Ce(NO_3)_3 \cdot 6H_2O$,

* *Present address*: Universidade Federal de Sao Carlos, DEMa, C.P. 676, CEP13560, Sao Carlos, S.P., Brazil.

0022–2461/90 $03.00 + .12

kept at pH = 3 with acetic acid. Under such conditions the alkoxides coprecipitate and the cerium nitrate remains in solution. The pH of the solution was adjusted to 10 by adding NH_4OH at which point the cerium compound was precipitated homogeneously throughout the small zirconium : titanium agglomerates. The precipitates were washed three times with isopropyl alcohol after separation from the liquid. After drying, the powder was calcined at 950° C for 30 min and subsequently ball milled in an alcohol medium. The calcination programme was based on the results of thermogravimetric and differential analysis. Powders were uniaxially pressed into discs at 190 MPa and sintered at temperatures in the range 1300 to 1600° C for 2 h. The sintering behaviour of green compacts under isothermal conditions in air, at temperatures of 1300 and 1350° C, was investigated using a sintering dilatometer.

Phase analysis of the sintered discs was performed using X-ray diffraction (XRD) and transmission electron microscopy (TEM). X-ray diffraction measurements were made using a Philips PW diffractometer with nickel-filtered copper radiation. The volume fraction of monoclinic and tetragonal phases present were calculated using Toraya *et al.* equation [11], assuming $P = 1.31$. Samples for transmission electron microscopy were prepared by ion-beam thinning in the conventional manner. TEM was carried out on a Jeol 200CX(STEM) operated at 200 kV and fitted with a Link EDS detector. A Philips 430 operated at 300 kV was used for high-resolution microscopy and convergent-beam diffraction.

Quantitative microanalysis was obtained using both an electron probe microanalyser (EPMA) and TEM. EPMA was conducted on a Jeol JX50A using high-purity ZrO_2, CeO_2, TiO_2 samples as standards. For quantitative TEM microanalysis, the Cliffe–Lorrimer ratio technique [12], which relates the X-ray intensity to the specimen composition, may be used, defined as

$$\frac{C_A}{C_B} = K_{AB}\frac{I_A}{I_B} \quad (1)$$

where C_A, C_B are the true concentrations of element A or B in the material, I_A, I_B are the integrated intensities of the relevant X-ray peak for the constituent element A or B, and K_{AB} is the Cliffe–Lorrimer factor.

The equation above only applies where "thin foil criteria" are met, i.e. where no absorption of X-ray occurs in the foil [13–16]. To determine whether absorption is a problem in this material, point analyses were made for a range of foil thicknesses, and the integrated intensities (with background subtracted) were plotted against foil thickness (the foil thickness was determined by measuring the spacing between carbon deposits after tilting the specimen). No significant change in integrated intensity with foil thickness was detected for either the titanium or cerium peaks and therefore absorption correction was not needed.

The Cliffe–Lorrimer factors were determined using the thin foil as the standard [16]. A thin foil was prepared from a sintered disc for which the chemical analysis had been determined accurately by EPMA and X-ray fluorescence (XRF). EPMA was unable to detect any segregation across any of the grains. Fifteen individual analyses were recorded from different grains, each from the same foil thickness. Long counting times were employed to minimize errors. Background radiation was removed from the integrated intensity using a program supplied with the Link system. From this work, Cliffe–Lorrimer factors of $K_{ZrCe} = 1.590 \pm 0.030$ and $K_{ZrTi} = 0.915 \pm 0.018$ were determined. All subsequent quantitative analyses were made, wherever possible, on the same foil thickness as that used in the determination of the Cliffe–Lorrimer factors.

TABLE I General properties of 77.9 ZrO_2 · 16.5 TiO_2 · 5.6 CeO_2 mol % composition

	Temperature (° C)					
	1300	1350	1400	1450	1500	1600
Density ($g\,cm^{-3}$)	5.40	5.88	5.87	5.81	5.52	5.31
Grain size (μm)	0.9	2.7	5.0	8.0	16.6	36.0
Tetragonal phase (vol %) (as-sintered surface)	100	100	100	97	8	2

The average grain size was determined by a linear intercept method [17] using scanning electron micrographs (observed on a Hitachi S700) of thermally etched surfaces. Tetrakiadecahedrally shaped grains with a log-normal size distribution was assumed and between 800 and 1000 grains were used to obtain an average. Fracture toughness measurements were made using the indentation technique with data being obtained as a function of load [18].

3. Results and discussion

3.1. Sintering behaviour in the temperature range 1300 to 1400° C.

The density as a function of sintering temperature is shown in Table I. Full densification was achieved in the temperature range 1350 to 1400° C, with tetragonal zirconia being the only crystalline phase detected. The microstructure consisted of fine equiaxed grains, Fig. 1. Sintering dilatometer traces, presented in Fig 2, suggest that densification occurs by a liquid-phase sintering mechanism at temperatures of 1350° C and above. The presence of a liquid phase at this temperature might be associated with the TiO_2 · CeO_2 phase diagram where $CeTi_2O_6$ is the only phase formed and melts incongruently at 1365 ± 5° C [19]. TEM of discs sintered in the range 1350 to 1450° C revealed an occasional pocket of glassy phase at triple points confirming that liquid-phase sintering had occurred, Fig. 3. Although the amount of glass phase found was small, it was comparable to the levels found in many zirconia–ceria and zirconia–yttria TZPs [20] (although levels in these materials can be much higher). The apparent absence of a glass phase at many grain boundaries and triple points may be due to the recombination of the glass-forming constituents into the matrix during cooling from sintering [21].

TEM microanalysis of the glassy pockets suggests that the composition of the amorphous phase is similar to that of the matrix, although the pockets found in the TEM were too small to allow accurate

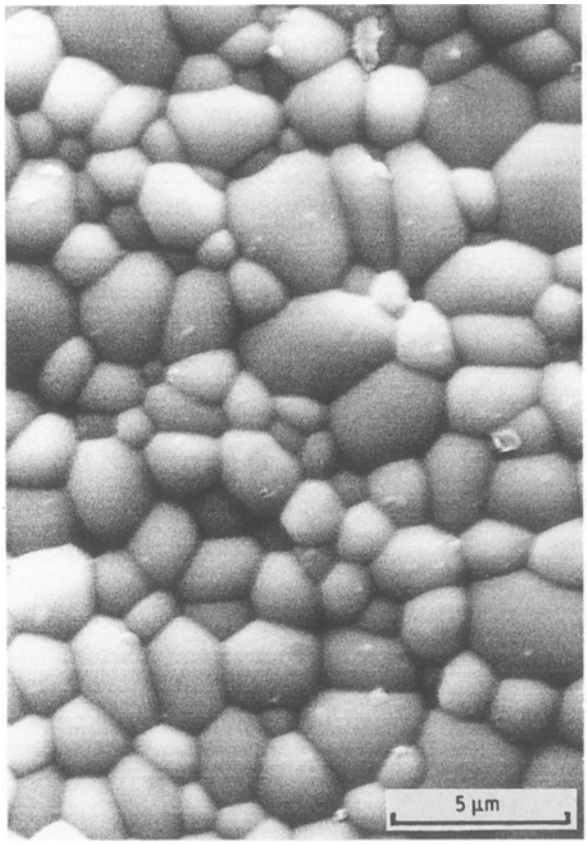

Figure 1 Scanning electron micrograph of a thermally etched surface from the sample sintered at 1350° C.

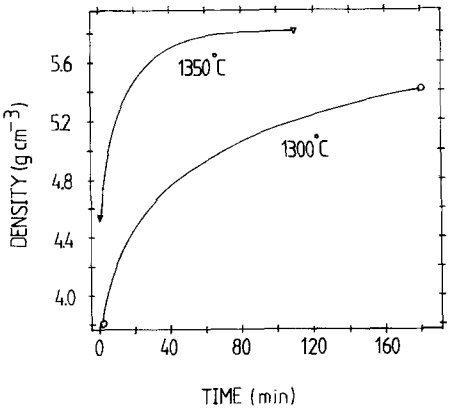

Figure 2 Sintering dilatometer trace showing density as a function of time for samples sintered at 1300 and 1350° C. Curves represent the best fit to 50 data points.

analysis. Moreover, because the oxygen content could not be determined, great care in calculating fully quantitative ratios is needed [16]. EPMA failed to detect any intergranular phase at 1350° C. At 1400° C the few areas large enough to allow microanalysis suggested an approximate doubling of the original concentration of TiO_2 and a slight decrease in the CeO_2 level compared to the matrix. Here again, the second-phase pockets were too small to avoid any matrix contribution to the measured value. Any loss of stabilizer to the glass phase was too small to be detected in analysis of the matrix, which retained the same ratios of the constituents as that of the starting powder.

The grain size of the tetragonal phase increased markedly with temperature, see Table I. This change in grain size was accompanied by an increase in thermal mismatch stresses which caused quite extensive microcracking along the grain boundaries in the larger grain-sized materials, see Fig. 4. Despite these large residual stresses, the tetragonal phase formed at 1350° C was remarkably stable and resisted any transformation to the monoclinic phase both after abrading the surface and even after plunging into liquid nitrogen.

The c/a ratio in the tetragonal phase was found to be 1.0327 $\pm$ 0.0001 in the discs sintered at 1350° C and 1.0284 $\pm$ 0.0001 in the powder calcined at 950° C. The tetragonality in the sintered material is significantly greater than in the zirconia–ceria and zirconia–yttria systems [22, 23]. The stability of the tetragonal phase appears to be associated with the high c/a ratio, the reasons for which are discussed in detail in Section 3.3.

3.2. Characterization in the temperature range 1450 to 1600° C

Table II gives the phase analysis determined by X-ray measurements on the as-sintered surfaces. The small amount of monoclinic phase detected in the sample sintered at 1450° C could not be found in TEM foils, but this was only considered to be a sampling effect. Although X-ray diffraction suggested tetragonal (t) and monoclinic (m) to be the only phases present, small amounts of $ZrTiO_4$ were also found using TEM,

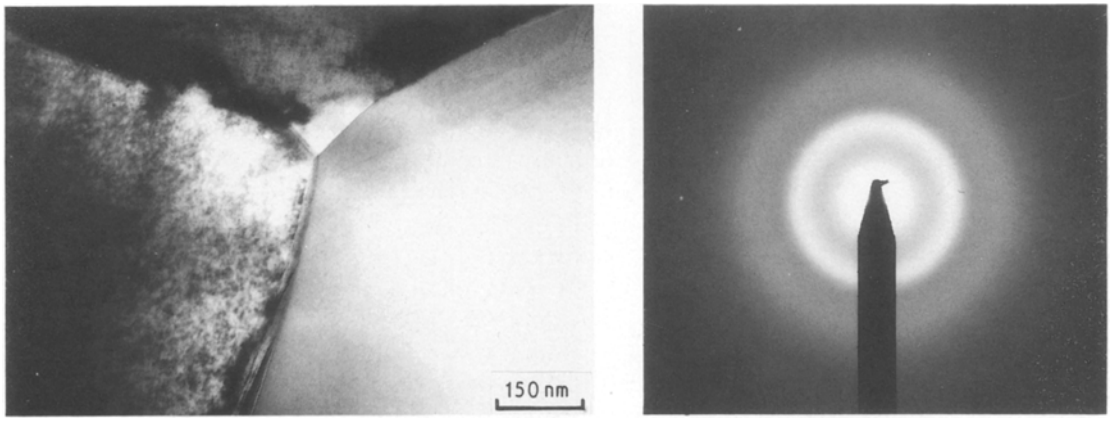

Figure 3 Transmission electron micrograph of the sample sintered at 1350° C showing a small pocket of an amorphous phase at a triple point.

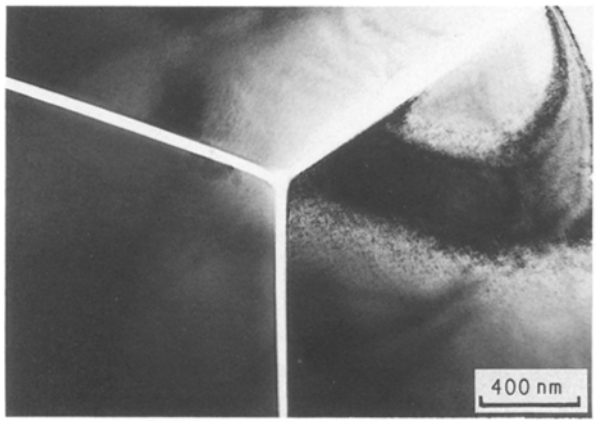

Figure 4 Transmission electron micrograph of the sample sintered at 1350° C showing thermal expansivity mismatch microcracks. Imaged under multibeam conditions.

Fig. 5. No loss of stabilizer from the tetragonal phase to the zirconium titanate in the region adjacent to the second phase could be detected and the composition of the tetragonal phase was the same as that of the bulk matrix. Small ellipsoid features, rich in cerium and titanium, were found on the sintered surface (Fig. 6). These are considered to have formed as a result of the liquid phase moving out of the sample by capillary action during sintering and collecting on the surface. This would suggest that an increase in the quantity of liquid phase occurred over and above the 1400° C sample, although this could not be detected in the TEM. Because the matrix composition was found to be the same as that in the 1350 to 1400° C samples, Table III, loss of stabilizer to the glass phase and zirconium titanate must be minimal. Nonetheless, a small drop in density had occurred, Table I, which is believed to be associated with the formation of monoclinic phase and the increase in grain-boundary microcracking from the increased grain size.

Samples sintered at 1500° C showed a dramatic change in microstructure with substantial quantities of monoclinic phase and zirconium titanate present, Table II. In addition, $Ce_2Zr_2O_7$ was found on the sintered surface by XRD, and a ceria-rich phase was identified on polished sections, Fig. 7. A substantial increase in the amount of glass phase was observed,

TABLE II Evolution of phase content (arbitrary units) with sintering temperature for the 77.9 ZrO_2 · 16.5 TiO_2 · 5.6 CeO_2 mol % composition

Phase	1300° C	1400° C	1450° C	1500° C	1600° C
ZrO_2 (t)	100	100	97.4	8.0	2.1
ZrO_2 (m)	–	–	2.6	68.2	85
$ZrTiO_4$	–	–	–	16.8	6.8
$Ce_2Zr_2O_7$	–	–	–	7.0	6.0

with a thin film along the majority of grain boundaries which congregates at triple points. Considerable amounts of the liquid phase had capillarated out of the sample and collected on the sintered surface.

The amorphous phase contained high levels of cerium and titanium, as well as zirconium (Table IV). As noted earlier, the absolute values of the elements may be slightly different from those given in Table IV, because the exact oxygen content could not be determined and may well be different to that in the material used as a standard. However, it is clear that the levels of cerium and titanium in the glass varied considerably.

The loss of stabilizer from the matrix to the second phases was clearly shown in the analysis of the tetragonal and monoclinic phases by TEM (see Table III), although the EPMA results are less conclusive because of the large area sampled. This phase separation was clearly responsible for the large increase in the amount of monoclinic phase present. Interestingly, the fall in the amount of CeO_2 appears to have been more significant than loss of TiO_2. It was, perhaps, surprising that the levels of TiO_2 were only marginally lower than those in the starting powder given the high levels of titanium in the glass and the abundance of $ZrTiO_4$. Analysis of the tetragonal and the monoclinic phases showed a systematic difference in composition, in particular in the quantities of CeO_2, between the two. The monoclinic phase contained about half to two-thirds the level of CeO_2 than was present in the tetragonal phase. TEM of the material showed the monoclinic phase to be characteristically twinned (Fig 8), although the twin spacing was very much larger than found in, for example, the zirconia–ceria system. In many areas the monoclinic phase did not

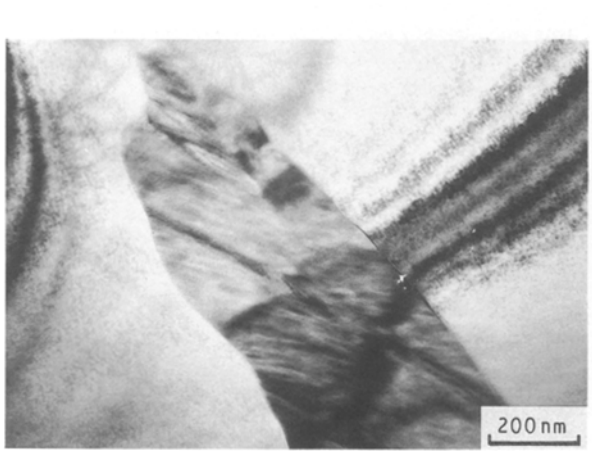

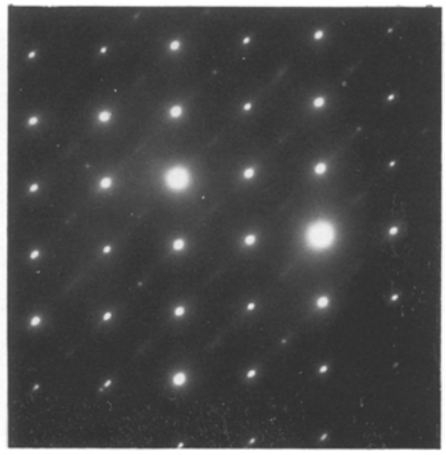

Figure 5 Transmission electron micrograph of a zirconium titanate pocket contained within a tetragonal zirconia grain. $B_{\text{Titanate}} = [1\,2\,1]$.

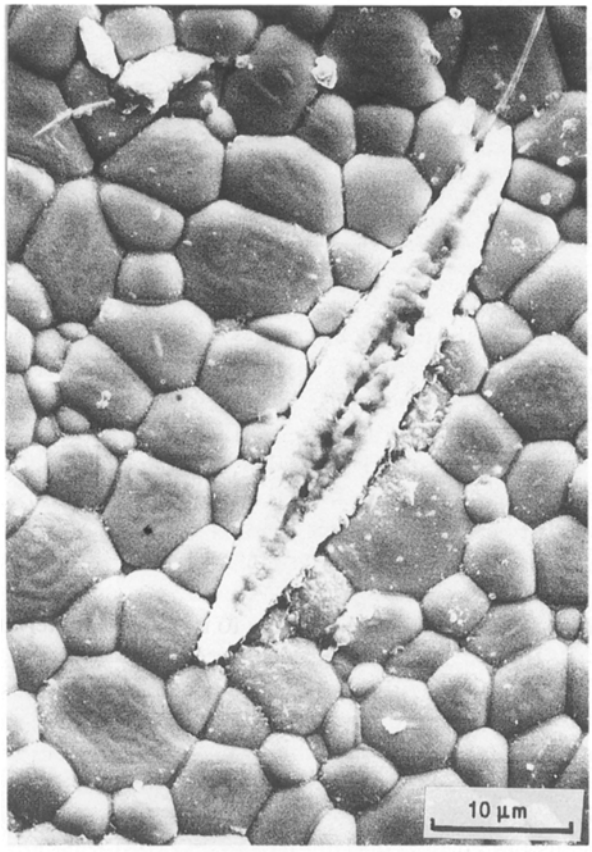

Figure 6 Scanning electron micrograph of the sintered surface of the 1450° C sample, showing one of many ellipsoid features, believed to be formed by capillaration of the liquid phase to the surface.

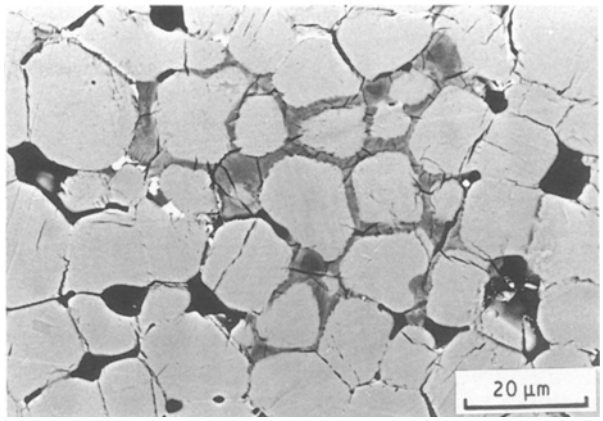

Figure 7 Scanning electron micrograph, using back-scattered electron imaging (BEI), of a polished section of the sample sintered at 1500° C. All grain boundaries are covered with a thick amorphous phase. The intergranular phase contains two crystalline phases, namely $Ce_2Zr_2O_7$ (white) and $ZrTiO_4$ (dark grey).

extend across an entire grain (Fig 9). This effect could also be seen on the sintered surface (Fig 10), suggesting that it was not associated with thin foil preparation. Clearly, therefore, despite the loss of stabilizer, the driving force for the t → m transformation was low. Microanalysis of the tetragonal and monoclinic phases where they coincided within a grain confirmed the monoclinic phase to be lower in CeO_2 than the tetragonal phase. Such levels of segregation are commensurate with the variable composition of the glass and the random distribution of the $ZrTiO_4$. The microanalysis results clearly indicate that the concentration of ceria is more important than the amount of titania, a result which is apparent from studies of the individual binary systems. These results do not, however, indicate the exact role of the ratio of the two stabilizers.

In the samples sintered at 1500° C, $ZrTiO_4$ regions were invariably surrounded by monoclinic or possibly a glassy layer. The thickness of the monoclinic layer was small, which infers that diffusion of the Ti^{4+} from the matrix to the $ZrTiO_4$ had only occurred over a short distance. This effect, however, demonstrates that titania does play a role in stabilizing the tetragonal phase. The analysis of the zirconium titanate showed a considerable variation in the ratios of Ti/Zr, with stoichiometry rarely being achieved. In the majority of cases the $ZrTiO_4$ contained appreciable amounts of cerium in solid solution (up to 5.6 mol %), which could act as a direct substitute for the Ti^{4+} in stabilizing the orthorhombic structure.

Regions rich in cerium and zirconium found on polished sections (Fig 11), were considered to be $Ce_2Zr_2O_7$ identified by XRD, although EPMA did suggest some titanium solubility in these particles. No evidence of the $Ce_2Zr_2O_7$ phase could be found in the thin foils. Investigation of the phases contained within the intergranular region was, however, extremely difficult because of preferential thinning during foil preparation.

The trend of increasing amount of liquid phase with temperature was continued in the sample sintered at 1600° C, as shown by the back-scattered electron image in Fig. 11. The thickness of the intergranular phases was so large that gravitation and capillary action had caused a considerable amount of the liquid to fall out of the sample during sintering. As a result of this, and the high monoclinic levels, with its associated microcracking, the sample had a very low density and mechanical strength (Table I). The loss of stabilizer from the matrix to the liquid and to other phases such as zirconium titanate is clearly demonstrated by

TABLE III Electron microprobe analysis (EPMA) and TEM microanalysis for the main matrix phase. (t = ZrO_2 tetragonal, m = ZrO_2 monoclinic, s = standard composition)

Temperature (° C)	EPMA (mol %)			TEM (mol %)		
	ZrO_2	TiO_2	CeO_2	ZrO_2	TiO_2	CeO_2
1350	77.22 ± 0.25	16.96 ± 0.12	5.80 ± 0.13	t(s): 77.22	16.96	5.80
1400	76.87 ± 0.20	17.08 ± 0.70	6.05 ± 0.13	t: 76.84–77.60	16.75–17.14	5.65–5.99
1450	77.67 ± 0.08	16.51 ± 0.03	5.82 ± 0.05	t: 77.60–77.82	16.68–16.75	5.49–5.65
1500	78.50 ± 0.63	15.91 ± 0.45	5.60 ± 0.18	t: 78.43–78.97	15.86–16.00	5.17–5.57
				m: 79.76–80.24	14.96–15.70	4.14–4.79
1600	83.30 ± 0.29	12.20 ± 0.25	3.95 ± 0.04	m: 84.83–86.74	7.95–11.10	2.16–3.27

TABLE IV Intergranular phase composition (EPMA) and glass analysis (TEM) with sintering temperature

Temperature (°C)	EPMA (mol %)			TEM (mol %)		
	ZrO_2	TiO_2	CeO_2	ZrO_2	TiO_2	CeO_2
1400	60.35 ± 1.22	34.77 ± 1.07	4.87 ± 0.15	74.81	18.47	6.73
1450	49.39 ± 0.15	45.77 ± 0.15	4.86 ± 0.16	75.44	17.47	6.70
1500	26.7–59.9	32.8–57.6	7.3–15.7	67.14–71.16	18.06–21.40	10.78–11.46
1600	3 distinct regions (see Fig. 15)			60.25–69.32	11.87–29.45	10.52–18.81

the EPMA results in Table III. Close examination in the SEM of the thick boundary films suggested that the liquid segregated into Zr/Ti rich inclusions as well as Ce/Zr particles (believed to be $Ce_2Zr_2O_7$) leaving the remainder of the intergranular phase rich in Ti/Zr (Fig. 11 and Table IV). TEM foil preparation of such a friable material proved very difficult. Whilst foils were prepared, they did not permit further investigation of the nature of the inclusions. Those areas of glass which were observed were single phase and of a composition similar to that found in the 1500° C samples, Table IV. In addition to the phases identified by X-ray analysis, small pockets of TiO_2 were found in thin foils (Fig. 12).

The structure of the zirconium titanate was analysed in detail in these samples where the size of the inclusion made its study practicable. The structure was extensively twinned, as shown by the spot splitting in the diffraction pattern (Fig. 13). Diffraction spots from planes of wide spacing (up to 0.73 nm) in Fig. 13 could only be attributed to an ordered structure. Dark-field images from the diffraction pattern indicated that the superlattice spots were only generated from alternating twins and that a very fine substructure existed within the ordered regions (Fig. 13).

Lattice fringe images were readily generated from these superlattice spots (Fig. 14). Distortion of the superlattice fringes is considerable with such irregularities coinciding with the "micro-domains" identified in the dark-field images. Whilst superlattice fringes were visible only in alternating twins for this orientation, tilting the sample confirmed that the entire region was ordered. The structure of the zirconium titanate was clearly complex, and there was some evidence that the morphology of the titanate varied within the sample, a result which would be expected due to the compositional variation found.

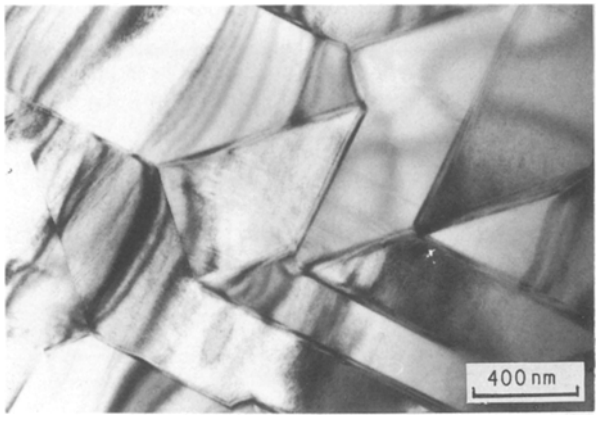

Figure 8 Transmission electron micrograph of the monoclinic phase showing a wide twin spacing, imaged under multibeam conditions.

The changes in phase stability with sintering temperature in the range 1350 to 1600° C, are complex. In order to summarize the phase segregation described in the previous two sections, all the results of the microanalysis measurements from the EPMA are plotted on a ternary diagram in Fig. 15. This clearly demonstrates (i) the loss of stabilizer from the zirconia matrix to the liquid phase and to other phases, and (ii) the phase separation within the intergranular phase at the higher sintering temperatures.

3.3. Stability of tetragonal zirconia

The tetragonal zirconia polycrystals formed in this study were found to be remarkably resistant to transformation to the monoclinic phase. Table V lists the fraction of monoclinic phase measured for the sample sintered at 1350° C after various treatments designed to initiate the t → m transformation. No transformation could be detected even after plunging into liquid nitrogen, and only a small amount of transformation occurred after fragmentation of the sample in a shatter box. The absence of transformation was clearly responsible for the low strength and toughness levels measured (Table VI). An increase in toughness was only obtained by considerable grain growth to 7.8 μm after ageing samples for 64 h at 1350° C. This increased the transformability as shown by Table V, approximately doubling the fracture toughness (Table VI).

The stability of the tetragonal zirconia was not simply a grain-size effect as demonstrated by the incomplete transformation across a grain and the wide twin spacing in samples sintered in the temperature range 1500 to 1600° C, even where the grain size was large and considerable loss of stabilizer had occurred (see Figs 8 and 9). In none of the foils examined could the t → m transformation be initiated by electron-beam heating, even in the 1450° C sample, which had a grain size of 8 μm. The reasons for the stability of the tetragonal phase are clearly important because they could provide additional evidence for the factors

TABLE V Monoclinic volume fraction (%) for the 77.9 ZrO_2 · 16.5 TiO_2 · 5.6 CeO_2 mol % subjected to different thermal and surface treatment

	As-sintered surface	Ground surface	Fracture surface	Shatter box*	Liquid N_2†
1350° C (2 h)	0	0	0	9	0
1350° C (64 h)	5	25	30	60	94

*XRD after milling for 10 min in a WC shatter box.
†XRD of the sample surface after being plunged for 5 min in liquid nitrogen.

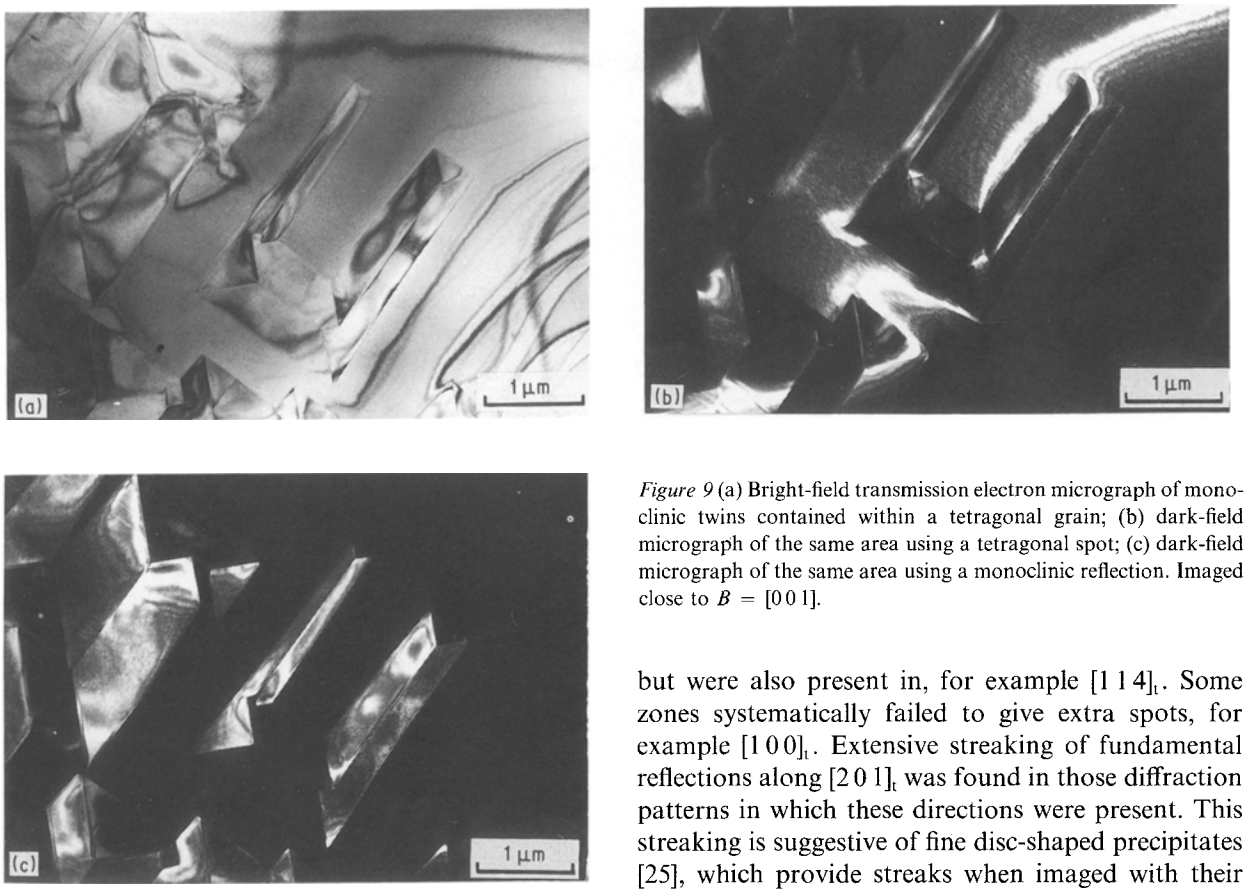

Figure 9 (a) Bright-field transmission electron micrograph of monoclinic twins contained within a tetragonal grain; (b) dark-field micrograph of the same area using a tetragonal spot; (c) dark-field micrograph of the same area using a monoclinic reflection. Imaged close to $B = [0\,0\,1]$.

controlling the transformability of the commercially important TZPs (e.g. the ceria-doped system). The low transformability in this system is surprising considering the levels of CeO_2 and TiO_2 and given the stability of the tetragonal phase in the binary systems, as noted earlier. In the zirconia–titania system the tetragonal phase cannot be retained to room temperature for sintered pellets [7]. In the zirconia–ceria case the tetragonal phase is highly transformable for a grain size of about 3 μm, with very high toughness values recorded through the formation of large transformation zones by the action of autocatalytic transformation [24]. The high stability of the tetragonal phase in this ternary system is therefore unexpected.

When examined in the TEM the tetragonal grains showed a fine-scale mottled structure (Fig. 16), which was present with the same contrast in samples sintered in the temperature range 1350 to 1450° C and at higher temperatures where the tetragonal-phase existed. The mottling appeared to be associated with the presence of extra spots in the diffraction pattern. These "superlattice" spots were invariably strongest for $[1\,1\,2]_t$ perpendicular to the foil surface, as shown in Fig. 16,

TABLE VI Mechanical strength (σ) and indentation toughness (K_{Ic}) for the 77.9 ZrO_2 · 16.5 TiO_2 · 5.6 CeO_2 mol % sintered at 1350° C

Sintering condition	σ* (MPa)	K_{Ic} (MPa $m^{0.5}$)
1350° C (2 h)	362 ± 35	5.8 ± 0.4 (5 kg†), 4.6 ± 0.4 (15 kg)
1350° C (64 h)	–	8.2 ± 0.4 (10 kg), 8.6 ± 0.6 (20 kg)

*Measured by four-point-bend stress.
†Indentation load utilized.

but were also present in, for example $[1\,1\,4]_t$. Some zones systematically failed to give extra spots, for example $[1\,0\,0]_t$. Extensive streaking of fundamental reflections along $[2\,0\,1]_t$ was found in those diffraction patterns in which these directions were present. This streaking is suggestive of fine disc-shaped precipitates [25], which provide streaks when imaged with their thin dimension parallel to the beam direction. The one exception found in the diffraction patterns to this was streaking along $[0\,4\,1]_t$. However, because (0 4 1) and (0 2 1) are separated by only 10° this streaking is probably also from $[2\,0\,1]_t$ rather than $[0\,4\,1]_t$. Additional

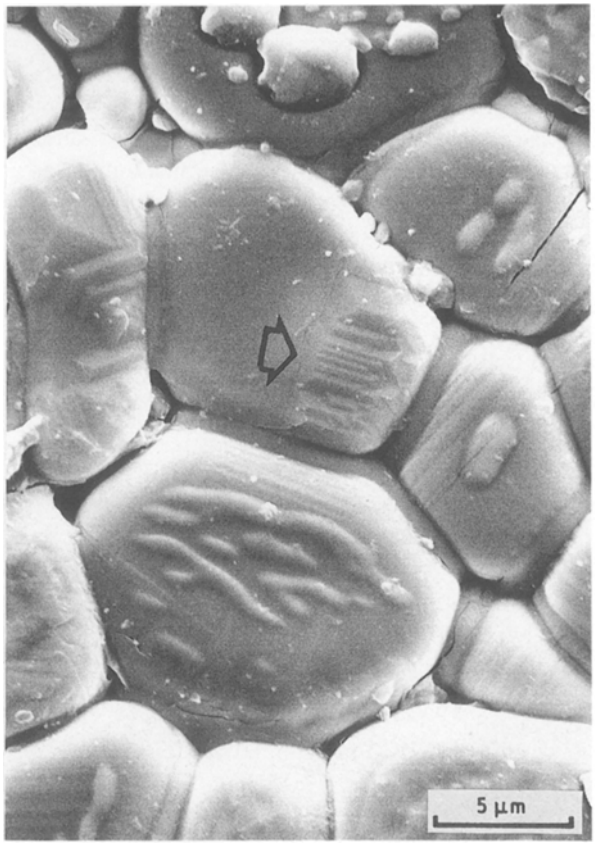

Figure 10 Scanning electron micrograph of the sintered surface of the 1500° C sample, showing incomplete transformation of t → m in the central grain (arrowed).

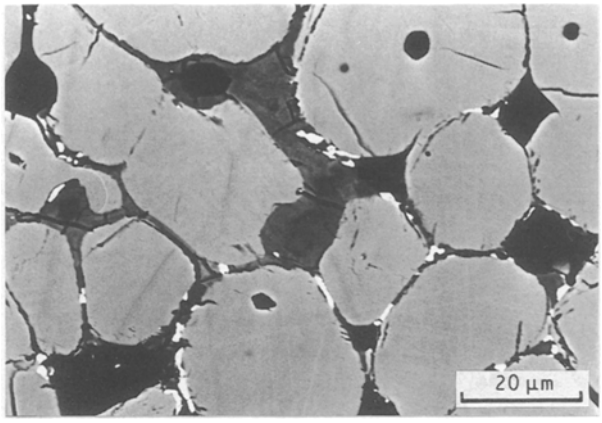

Figure 11 BEI micrograph of a polished section of the sample sintered at 1600° C. The sample shows similar features to Fig. 7, except there are greater quantities of $Ce_2Zr_2O_7$ (white) and $ZrTiO_4$ (dark grey) and the grain size is considerably larger.

weak peaks were found in the XRD data, which could not be explained as being due to any of the possible primary phases in this system, with one peak corresponding approximately to the $1/2(2\,0\,1)_t$ reflection in Fig. 16. There were insufficient peaks present in the trace, however, to determine the crystallography of this particular diffracting phase.

Dark-field imaging of the mottled structure using the precipitate spots failed to differentiate clearly the regions giving rise to the extra spots (Fig. 16). This was due to the extremely fine nature of the microstructure and the weakness of the extra spots occurring in regions of the foil which were thin enough to give a clear image (the strongest spots were invariably obtained from thicker regions of the foil).

Bestgen *et al.* [9] have recently reported a similar mottled structure in an 8 wt% Y_2O_3 PSZ. In their work the mottling was most prevalent in grains where the $[1\,0\,0]_t$ axis was perpendicular to the foil surface, and was usually at its strongest immediately prior to the electron-beam heating-induced transformation of $t \rightarrow m$. They associated the mottling with low-intensity "superlattice" spots in the $[1\,0\,0]_t$ diffraction pattern, indicating monoclinic or orthorhombic (o) symmetry, and identifying it as a thin foil effect, caused by the lack of surface constraint, which could not occur in the bulk material. Urabe *et al.* [10] have also found a mottled structure in a $4CeO_2 \cdot 4YO_{1.5} \cdot 92ZrO_2$ TZP, which they attributed to microdomains of monoclinic or orthorhombic phases. The mottling could be made to disappear by heating the foil. In a $20CeO_2 \cdot 80ZrO_2$ sample no mottling could be found which was explained by the low A_s (starting temperature for the monoclinic → tetragonal zirconia transformation on heating) temperature in this material, which, therefore, supports the findings of Bestgen *et al.* [9].

Otsuka *et al.* [26] also found extra reflections which were associated with a mottled structure in Cu–Al–Ni alloys, which could also be considered to be a similar "premartensitic" behaviour. The extra reflections were strong for [1 1 2], and sometimes present in [1 1 3] and [0 0 1], but not reproducibly so. Otsuka *et al.* found that the mottling disappeared on heating the specimen and considered that it arose from small precipitates of a "2H" structure. However, mottling was subsequently inhereted by the martensitic phase, indicating that the mottling was not premartensitic behaviour.

In the present study mottling was present even in the 1350° C sample where no transformation from tetragonal to monoclinic phase could be induced by plunging into liquid nitrogen, which therefore suggests an alternative explanation to that of Bestgen *et al.* [9] is required. Moreover, the crystallography of the mottling appears different from that described by Bestgen *et al.* [9], although information from an $[1\,0\,0]_t$ was the only zone given by these authors. In the present case, no "superlattice" spots were observed for $[1\,0\,0]_t$. Furthermore, the mottled structure was inhereted by the monoclinic phase. A more probable explanation for the present results is that some form of short-range order is occurring. The ordering would conveniently explain the large c/a ratio of the tetragonal phase, which, as noted earlier, was found to be larger than normally expected from the binary systems. The c/a ratio had increased in the sintered product compared to the powder, a phenomenon which can be explained by the development of ordering during sintering. Additionally, the presence of short-range order would be expected to contribute to the stability of the tetragonal, as was found in this material. In order to prove the presence of an ordered lattice, attempts were made to form a lattice fringe image from the superlattice reflections. These reflections were found to be too faint in regions where the foil was

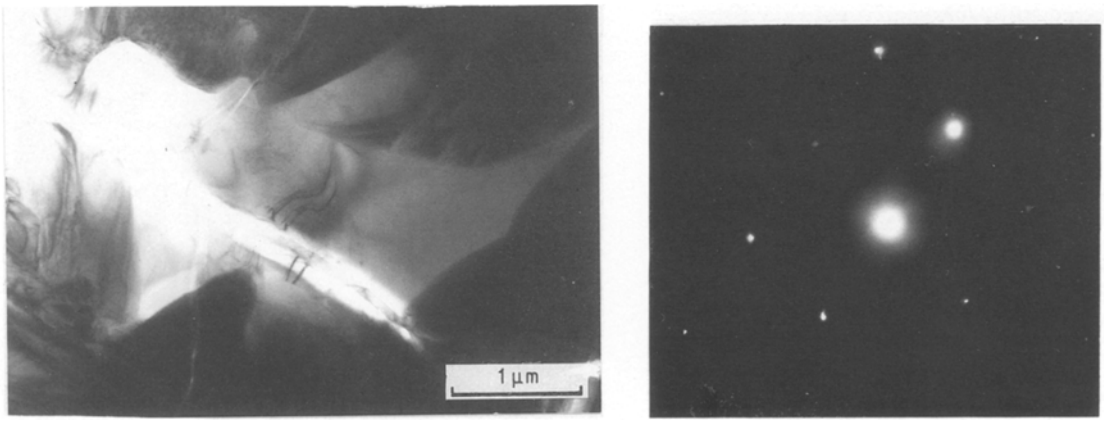

Figure 12 Transmission electron micrograph of an isolated pure TiO_2 particle. B is close to [0 1 1].

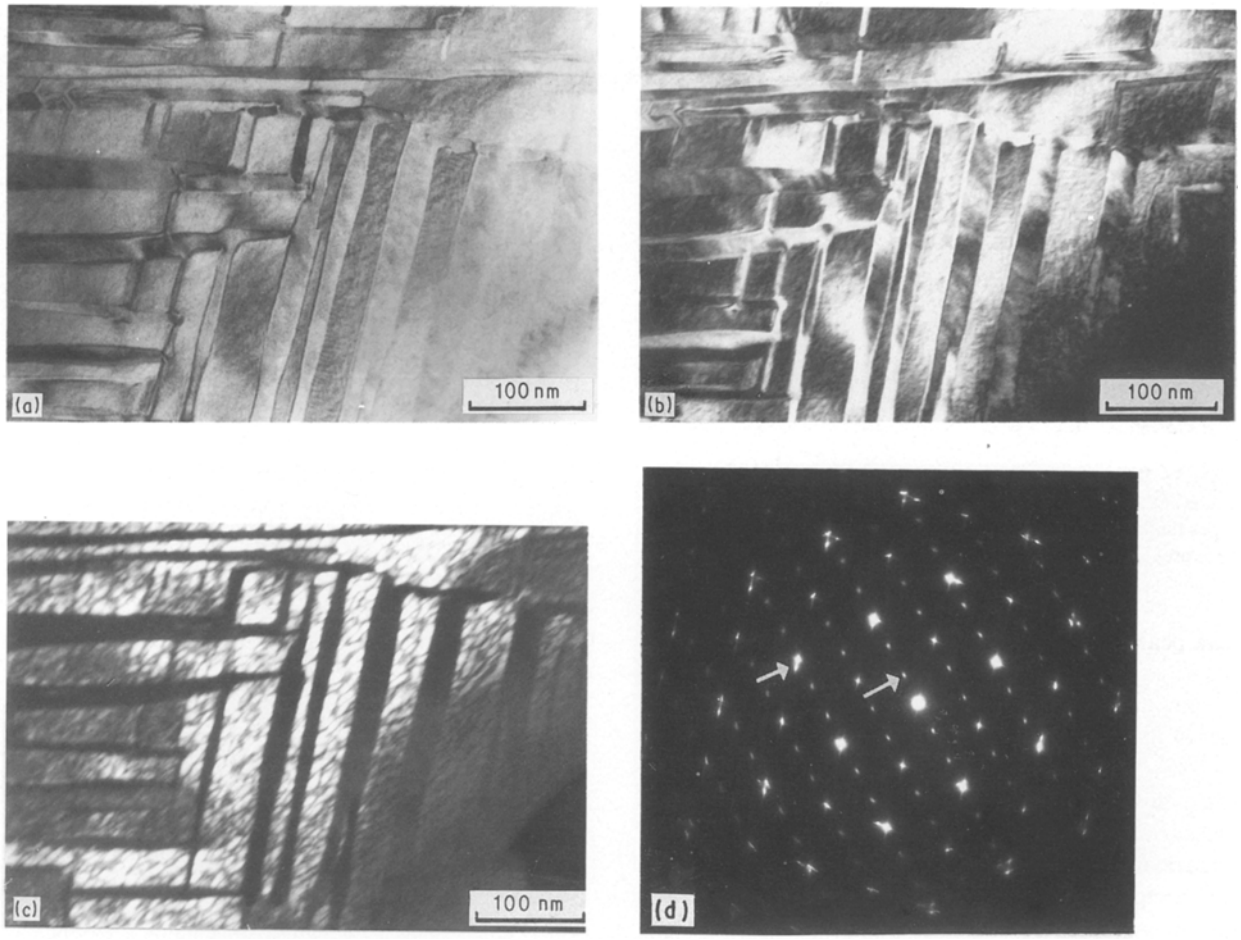

Figure 13 (a) Bright-field micrograph of a heavily twinned zirconium titanate particle; (b) dark-field micrograph of the same area using a fundamental diffraction spot; (c) dark-field micrograph of the same area using a superlattice diffraction spot, showing a very fine structure to the ordered lattice; (d) selected-area diffraction pattern from this area, $B = [0\,0\,1]$, with the diffraction spots used for the dark fields arrowed.

thin enough to give phase contrast and only fringes derived from the tetragonal lattice could be imaged.

Anti-phase domain boundaries (APB) were frequently observed in the monoclinic phase formed in the 1500 and 1600° C samples. The APBs, Fig. 17, were similar to those found in the literature [9, 27] and indicated that the monoclinic phase was ordered. A lattice fringe image across an APB is presented in Fig. 18. The diffraction pattern from this region can be interpreted as $[1\,0\,0]_m$ or $[0\,0\,1]_m$ but also contains $(0\,1\,0)_m$ and $(0\,0\,1)_m$ forbidden reflections. Forbidden spots can occur by double diffraction, as demonstrated by Muddle and Hannink [28] for Mg-PSZ, but such an explanation appears improbable for the monoclinic phase with such a large twin spacing. A more likely explanation is that the $(0\,1\,0)_m$ and $(0\,0\,1)_m$ spots are

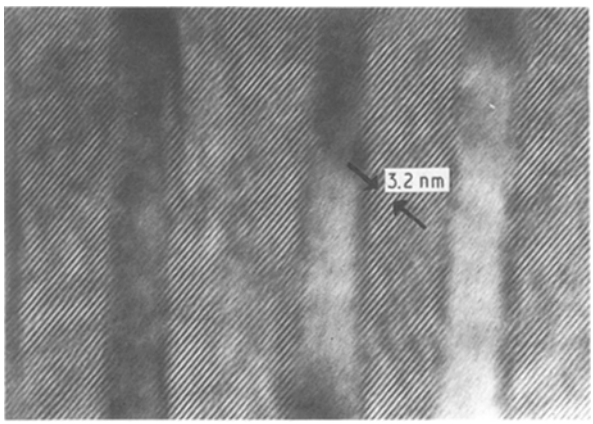

Figure 14 Lattice fringe image from the same orientation as Fig. 13. The objective aperture was centred on the transmitted beam and only included superlattice spots in the image.

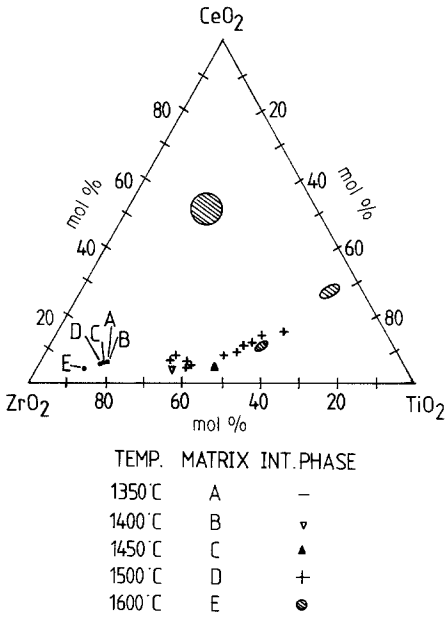

Figure 15 Ternary diagram from the EPMA results in Tables III and IV, showing the change in composition of the matrix and the intergranular phase as a function of temperature.

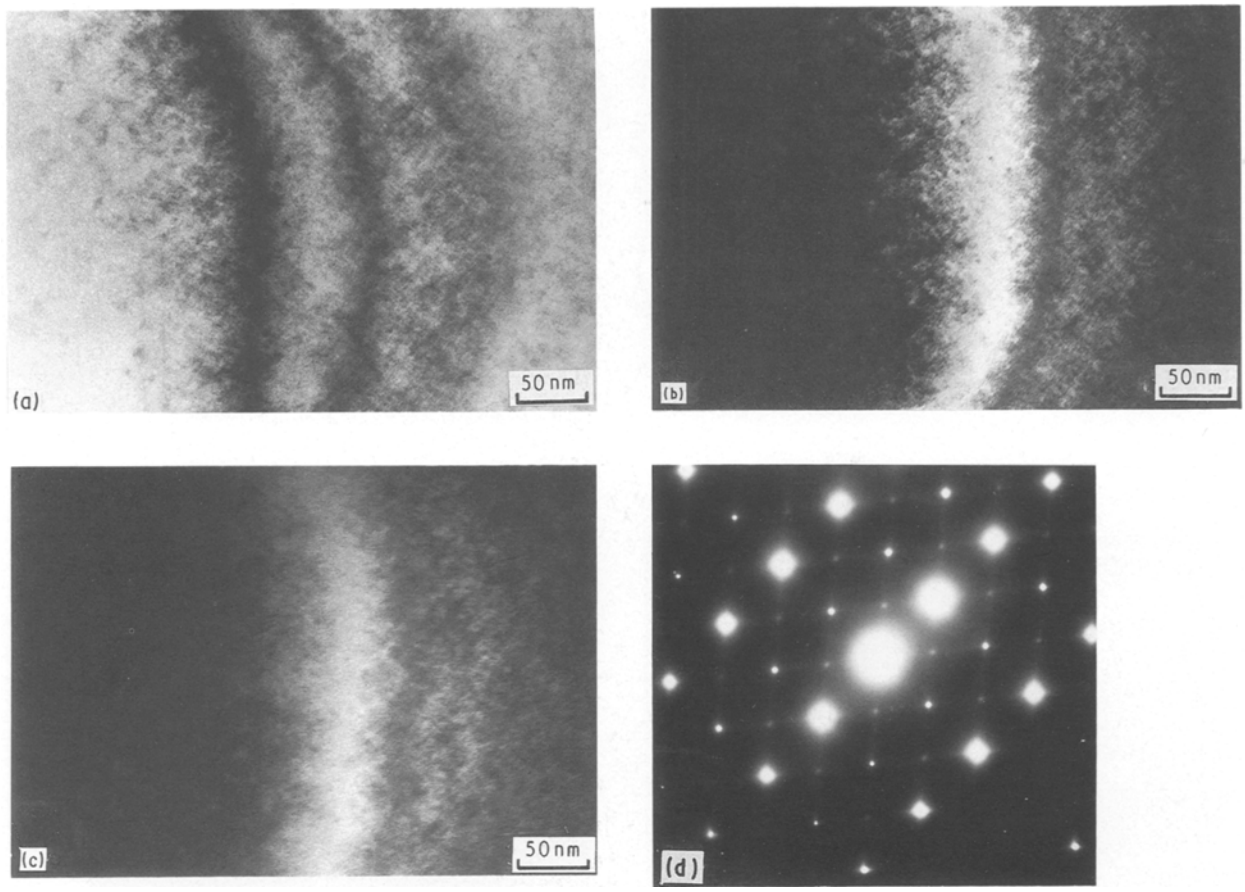

Figure 16 (a) Bright-field micrograph of the tetragonal phase in the 1350° C sample, showing a mottled structure on a very fine scale; (b) dark-field micrograph from the same area using a fundamental tetragonal diffracted spot; (c) dark-field micrograph of the same area using a superlattice reflection; (d) selected-area diffraction pattern for (a). B = [0 1 2], with superlattice spots at {1 1 0} and {2 0 1} and streaking along [2 0 1].

generated as a result of the superlattice. The lattice fringes in Fig. 18 show considerable distortion across the APB suggesting that they are derived from the ordered lattice rather than $(1\,0\,0)_m$.

Bestgen *et al.* [9] have demonstrated that the ordering is a result of the monoclinic phase being formed by transformation from an ordered orthorhombic phase. In their work the tetragonal phase was transformed by electron-beam heating to the orthorhombic (o) symmetry by a comparatively slow displacive transformation. The transformation front left APBs in its wake as it moved through the tetragonal phase. Transformation of o → m was induced by further electron-beam heating of the foil, with the resultant monoclinic phase retaining the APBs and the ordered structure. In those grains where t → m was induced directly, no evidence of ordering in the monoclinic was found. The orthorhombic phase has been found in many studies, for example in the Mg-PSZ system [29–31], the Ca-PSZ system [32] and the ternary Mg-Y-PSZ system [27]. In bulk samples, o-phase can only be detected at high pressure [33, 34] and at very low temperatures [9], and is generally considered to be an artefact of thin foil preparation when detected under ambient conditions.

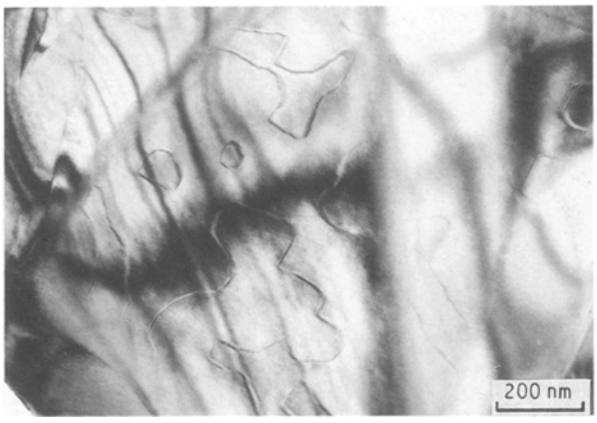

Figure 17 Transmission electron micrograph of an area of monoclinic phase containing APBs. Imaged under multibeam conditions.

In the present study the presence of ordering in the monoclinic is also believed to be a result of the formation of o-phase during thin foil preparation. Only small quantities of ordered monoclinic phase were discovered, invariably in thinner regions of the foil. The short-range order in the tetragonal phase would not be expected to provide long-range order in the monoclinic phase by a martensitic reaction. Indeed, the monoclinic phase which did not show any APBs exhibited the mottled contrast similar to that found in the tetragonal phase. An occasional pocket of a phase, with the same composition as the monoclinic and which contained APBs but was not twinned, was observed, (Fig. 19), which might be considered to be o-phase. Convergent-beam diffraction analysis indicated a rotational symmetry of 2 in both the whole pattern and the transmitted disc. This, therefore,

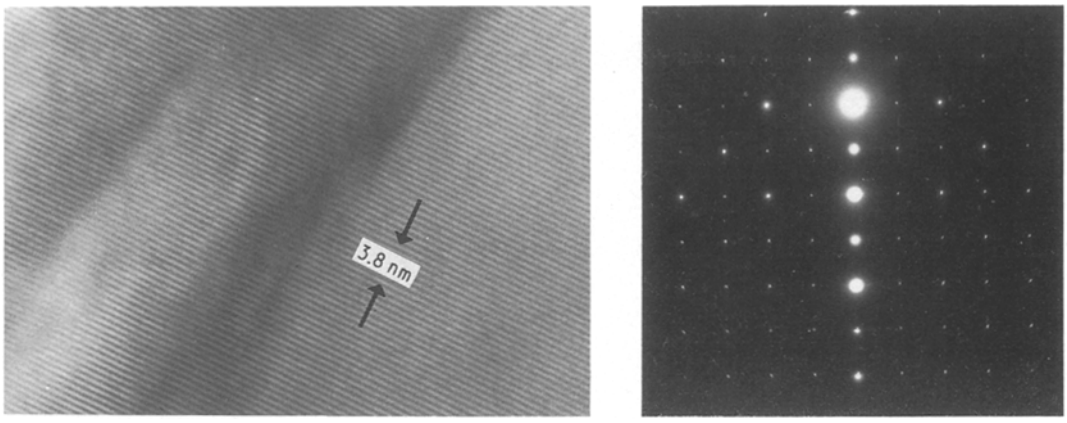

Figure 18 Lattice fringe image across an APB in a monoclinic twin. $B = [0\,0\,1]$, with the objective aperture centred on the transmitted beam, allowing only $\{1\,0\,0\}$-type reflection to form the image. See text for discussion.

indicates a diffraction group of 21_R, which occurs for monoclinic but not orthorhombic crystals. Whilst these pockets are clearly monoclinic, it is surprising that such a large area can exist without any twin boundaries. Faint additional spots are present in the diffraction pattern, corresponding to a lattice spacing of 0.64 nm, which must be derived from the ordering in the monoclinic phase.

4. Conclusions

This study has fully characterized the ternary composition $77.9ZrO_2 \cdot 16.5TiO_2 \cdot 5.6CeO_2$ (mol %) after sintering in the temperature range 1300 to 1600° C with the following conclusions.

1. Full densification to a totally tetragonal structure was achieved by liquid-phase sintering in the temperature range 1350 to 1400° C.

2. At sintering temperatures above 1450° C, loss of stabilizer from the matrix to the titanium-, cerium-rich liquid phase occurred. The liquid phase was fluid enough to capillarate to the sample surface, with losses being minimal at 1450° C but considerable at 1600° C. Additional loss of both titanium and cerium from the matrix resulted from the formation of zirconium titanate. An additional phase was formed, $Ce_2Zr_2O_7$, apparently by segregation within the intergranular phase. This became more pronounced at the higher sintering temperatures.

3. The tetragonal phase formed showed a high resistance to stress-assisted transformation to the monoclinic phase, which resulted in both low strength and toughness. Ageing a sample sintered 1350° C for 64 h at 1350° C produced appreciable transformation and an associated increase in toughness to about 8.4 MPa $m^{1/2}$. Even where considerable loss of stabilizer had occurred and where the grain size was large, complete t → m transformation did not occur, with transformation frequently being arrested half way across a grain. The stability of the tetragonal zirconia

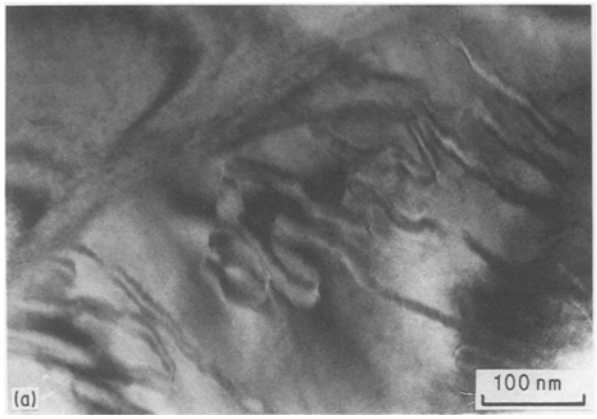

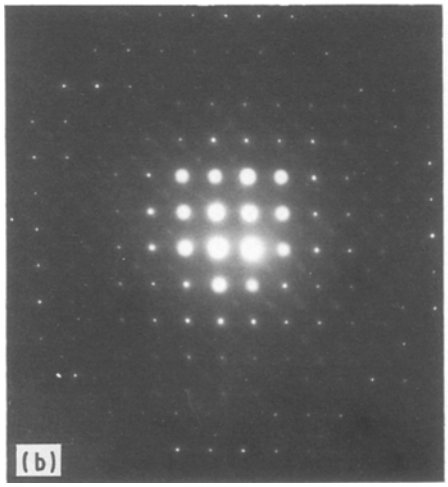

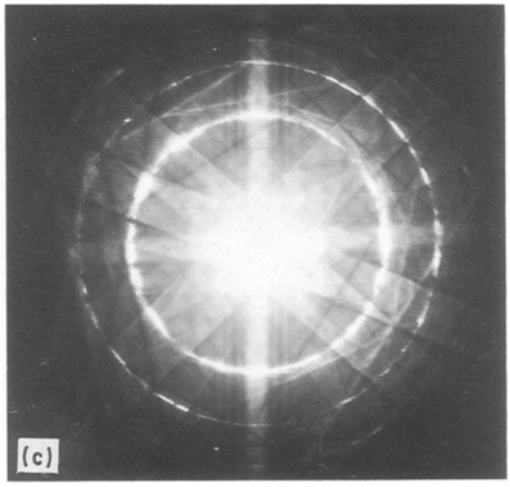

Figure 19 (a) Transmission electron micrograph of a small pocket of monoclinic phase which contains no twins. (b) Selected-area diffraction pattern, $B = [1\,2\,1]$, note the additional superlattice spots. (c) Convergent-beam diffraction pattern indicating a 21_R diffraction group.

appeared to be associated with the high c/a ratio measured for this material. The increased tetragonality is believed to be a result of short-range order in the tetragonal zirconia. The mottling was also inhereted by the monoclinic phase. It would appear that it is the combined effect of the TiO_2 and CeO_2 dopants which is important because ordering in the tetragonal phase has not been observed in the binary zirconia–ceria system.

Acknowledgements

The authors thank Dr C. Hammond and Professor R. J. Brook for helpful discussions. They also acknowledge receipt of CN P_q no. 2522/84-EQ by VCP and an SERC CASE studentship in collaboration with TI Research by M.R.

References

1. A. H. HEUER and L. W. HOBBS (eds), "Advances in Ceramics", Vol. 3, "Science and Technology of Zirconia 1" (American Ceramics Society, Columbus, Ohio, 1981).
2. N. CLAUSSEN, M. RUHLE and A. H. HEUER (eds), "Advances in Ceramics", Vol. 12 "Science and Technology of Zirconia 2" (American Ceramics Society, Columbus, Ohio, 1984).
3. S. SOMIYA, N. YAMAMOTA and H. YANAGIDA (eds), "Advances in Ceramics", Vol. 24, "Science and Technology of Zirconia 3" (American Ceramics Society, Westerville, Ohio, 1988).
4. J-G. DUH, H-T. DAI and B-S. CHIOU, *J. Amer. Ceram. Soc.* **71** (1988) 813.
5. E. TARNI, M. YASHIMURA and S. SOMIYA, *ibid.* **66** (1983) 506.
6. T. NOGUCHI and M. MIZUNO, *Bull. Chem. Soc. Jpn.* **41** (1968) 2895.
7. V. C. PANDOLFELLI, I. NETTLESHIP and R. STEVENS, in "Complex Ceramic Microstructure," edited by R. Stevens (British Ceramic Society, Stoke-on-Trent, 1989) p. 139.
8. V. LONGO and L. PODDA, *Ceramurgia* **4** (1974) 3.
9. H. BESTGEN, R. CHAIM and A. HEUER, *J. Amer. Ceram. Soc.* **71** (1988) 826.
10. K. URABE, A. NAKAJIMA, H. IKAWA and S. UDAGAWA, in "Advances in Ceramics", Vol. 24 "Science and Technology of Zirconia 3", edited by S. Somiya, N. Yamamoto, H. Yanagida (American Ceramics Society, Westerville, Ohio, 1988) p. 345.
11. H. TORAYA, M. YASHIMURA and S. SOMIYA, *J. Amer. Ceram. Soc.* **71** (1984) C183.
12. G. CLIFF and G. W. LORRIMER, in "Proceedings of the 5th European Congress on Electron Microscopy" (Institute of Physics, London, 1972) p. 203.
13. G. W. LORRIMER, G. CLIFF and J. N. CLARKE, in "Developments in Electron Microscopy and Analysis", edited by J. A. Venables (Academic Press, New York, 1976) p. 153.
14. N. J. ZALUZEC and H. L. FRASER, in "Proceedings of the 34th Annual Electron Microscopy Society of America" (Claitors, Baton Rouge, 1976) p. 420.
15. B. A. BENDER, D. B. WILLIAMS and M. R. NOTIS, *J. Amer. Ceram. Soc.* **63** (1980) 149.
16. D. B. WILLIAMS, in "Practical Analytical Electron Microscopy in Materials Science" (Philips Electron Optics, Verlag Chemie International, Amsterdam, 1984).
17. P. MENDELSON, *J. Amer. Ceram. Soc.* **52** (1969) 443.
18. G. R. ANSTIS, P. CHANTIKUL, B. R. LAWN and D. B. MARSHALL, *ibid.* **64** (1981) 553.
19. J. P. QUHA and D. KOLAR, *ibid.* **56** (1973) 5.
20. H. SCHUBERT, N. CLAUSSEN and M. RUHLE, in "Advances in Ceramics", Vol. 12, "Science and Technology of Zirconia 2", edited by N. Claussen, M. Ruhle and A. H. Heuer (American Ceramics Society, Columbus, Ohio, 1984).
21. R. J. BROOK, personal communication (1988).
22. K. TSUKUMA and M. SHIMADA, *J. Mater. Sci.* **20** (1985) 1178.
23. R. P. INGEL and D. LEWIS, *J. Amer. Ceram. Soc.* (1986) 325.
24. K. TSUKUMA, *Amer. Ceram. Soc. Bull.* **65** (1986) 1386.
25. G. THOMAS and M. J. GORINGE, in "Transmission Electron Microscopy of Materials" (Wiley, London, 1979).
26. K. OTSUKA, H. KUBO and C. M. WAYMAN, *Met. Trans. A.* **12** (1981) 595.
27. R. R. LEE and A. H. HEUER, *J. Amer. Ceram. Soc.* **71** (1988) 694.
28. B. C. MUDDLE and R. H. J. HANNINK, *ibid.* **69** (1986) 547.
29. A. H. HEUER, L. H. SCHOENLIEN and S. FARMER, in "Science of Ceramics 12", Saint-Vincent, Italy, edited by P. Vincenzini (Ceramurgica, Faenza, Italy, 1983) p. 257.
30. B. C. MUDDLE and R. H. J. HANNINK, in "Advances in Ceramics", Vol. 24, "Science and Technology of Zirconia 3", edited by S. Somiya, N. Yamamoto and H. Yanagida (American Ceramics Society, Westerville, Ohio, 1988) p. 89.
31. L. H. SCHOENLEIN and A. H. HEUER, in "Fracture Mechanics of Ceramics", Vol. 6, edited by R. C. Bradt, A. G. Evans, D. P. H. Hassleman and F. Lange (Plenum, New York, 1983) p. 309.
32. R. M. DICKERSON, M. V. SWAIN and A. H. HEUER, *J. Amer. Ceram. Soc.* **70** (1987) 214.
33. S. BLOCK, J. A. H. DAJORNADA and G. J. PIERMARINI, *ibid.* **68** (1985) 497.
34. Y. KUDOH, H. TAKEDA and H. ARASHI, *Phys. Chem. Mineral.* **13** (1986) 233.

Received 27 January
and accepted 24 August 1989